Asian Journal of Chemistry; Vol. 37, No. 11 (2025), 2803-2808
ASIAN JOURNAL OF CHEMISTRY
https://doi.org/10.14233/ajchem.2025.34618

Eco-friendly Synthesis of Silver Nanoparticles from *Persea americana*: Evaluation of Nonlinear Optical Behaviour and Antibacterial Efficacy

SUCHITHRA SUKUMARAN NAIR[1,2], VIJAYAKUMAR SADASIVAN NAIR[1,*], SARAVANA KUMAR[1], REMYA MURALIMANOHAR[1], HUBERT JOE[3] and ALICE NOBLE[4]

[1]PG and Research Department of Physics, N.S.S. College (Affiliated to University of Kerala), Pandalam-689501, India
[2]PG Department of Physics, St. Stephen's College (Affiliated to University of Kerala), Pathanapuram- 689695, India
[3]Department of Nanoscience and Nanotechnology, University of Kerala, Thiruvananthapuram-695581, India
[4]Department of Physics, University of Kerala, Thiruvananthapuram-695581, India

*Corresponding author: E-mail: vijayakumar@nsscollegepandalam.ac.in

Received: 3 August 2025 *Accepted*: 29 September 2025 *Published online*: 27 October 2025 AJC-22169

Plant-mediated synthesis of metal nanoparticles is widely employed for intended applications and is regarded as a dependable green method to reduce the use of hazardous chemicals. This study details a straightforward, economical and environmentally friendly method for synthesizing highly stable silver nanoparticles (AgNPs) using *Persia americana* (Avocado) leaf extract as both a stabilizing and reducing agent. Distinct peaks corresponding to the cubic silver crystallographic planes were confirmed by the X-ray diffraction (XRD) patterns. The surface plasmon resonance band of synthesized AgNPs was observed at around 452 nm using UV-Vis spectral analysis. FT-IR spectroscopy identified the plant extract's biomolecules responsible for the effective stabilization and reduction of AgNPs. Comprehensive nonlinear optical behaviour studies were conducted using a single-beam Z-scan setup with Nd: YAG laser source, revealing significant optical limiting properties with a threshold value of 5.97 J/cm^2. Furthermore, the prepared AgNPs demonstrated good antimicrobial effects against human pathogens, specifically *P. mirabilis*. These findings suggest that the as-synthesized nanosilver particles are promising candidates for optoelectronic devices and various antimicrobial applications.

Keywords: Silver nanoparticles, *Persia americana*, Z-scan, Optical limiting, Antibacterial activity.

INTRODUCTION

Metal nanoparticles, especially plasmonic nanoparticles, have emerged as an important group of nanosystems because of their wide applications in optics, plasmonics, biochemistry and biomedical applications including drug delivery, bioimaging and medical diagnosis. This is mainly due to the surface plasmon resonance (SPR) phenomenon shown by these particles [1,2]. The green chemistry approach uses plant extracts and microorganisms to synthesize metal nanoparticles. Since it is quick, easy, affordable, environmental friendly and produces a large amount of metal nanoparticles, it has become a viable, practical substitute for traditional physical and chemical methods [3-6]. Nowadays, synthesizing metal nanoparticles with plant extract is an easy way to produce nanoparticles on a big scale with less harm [7-12]. The environmentally benign, pure, economical and adaptable nature of nanoparticle biogenesis, which is frequently done at ambient temperature, makes it stand out. The use of biosynthesis is essential for preventing the development of dangerous or toxic byproducts, highlighting the necessity of simple and safe production methods. In practice, green synthesis of nanoparticles may be carried out effectively in ambient conditions and at a reasonable cost. A metallic salt solution is combined with a natural bio-reductant extract in a one-step synthesis procedure. Nanomaterials are rapidly created through the subsequent redox reaction, which requires relatively low initial energy. Consequently, rather than focusing on alternative synthesis methods, researchers specializing in nanoparticle synthesis have increasingly turned to plant extracts [13-17].

Among the various metal nanoparticles including gold, silver, platinum, *etc*., many researchers are interested in silver nanoparticles due to their wide applications in medicine, photonics, optoelectronics, catalysis, fabrication of nanodevices,

antimicrobial, biochemical sensing and so on [3]. Silver nanoparticles are one of the most promising materials among the plasmonic nanomaterials that have been investigated so far in nonlinear optical (NLO) investigations due to their remarkable optical capabilities that lead to well-known applications like optical switching and optical limiting [18,19].

The avocado plant was chosen for this research due of its numerous benefits. Avocado leaves are rich in bioactive compounds such as polyphenols, flavonoids, tannins and alkaloids, which act as natural reducing and stabilizing agents in the metallic nanoparticle synthesis [20]. Moreover, avocado (*Persea americana*) is widely cultivated, making its leaves an abundant and readily available byproduct. The strong antioxidant properties of the avocado leaves also enhance the stability of the synthesized nanoparticles [21]. Furthermore, silver nanoparticles derived from leaves demonstrate enhanced antimicrobial effects, which can be attributed to the combined action of silver and phytochemicals [22,23]. Hence, the primary emphasis of this investigation is the eco-friendly synthesis of silver nanoparticles utilizing *P. americana* (avocado) leaf extract. The structural, optical and nonlinear properties of silver nanoparticles were also investigated in this study.

EXPERIMENTAL

The analytical grade pure silver nitrate ($AgNO_3$) and the solvents was purchased from Sigma-Aldrich Chemicals, USA. Deionized water was used throughout the synthesis.

Preparation of leaf extract: Disease-free fresh avocado leaves were collected from the local garden of Kottarakkara, Kollam district, Kerala and subsequently washed using distilled water. Finely chopped fresh leaves (40 g) was then combined with 200 mL of distilled water and stirred at 70 ºC for 1 h. Following the boiling process, the mixture was allowed to cool and subsequently filtered using the Whatman filter paper of grade number 1. The resulting filtrate was collected and stored for further analysis.

Synthesis of silver nanoparticles: A 10 mL of leaf extract was added to $AgNO_3$ solution (0.04 M) with continuous stirring at room temperature. The colour change of the solution from yellowish-green to brown indicates that avocado leaf extract rapidly facilitates the biosynthesis of AgNPs at room temperature. The solution was kept under dark conditions, followed by an incubation period of 24 h. After centrifuging the resulting AgNPs the ROTEK M8E Laboratory Centrifuge at 5000 rpm for 10 min, the supernatant was discarded and the resulting precipitate was extensively washed with double distilled water followed by acetone to remove any unreacted particles. The refined sample collected was air-dried and used for further characterization.

Characterization: The XRD pattern of AgNPs powder was analyzed using a Panalytical Aeris Research edition X-ray diffractometer with Cu*K*α radiations (λ = 1.5418 Å) over the diffraction angle 2θ, between 10º and 80º. The surface plasmon resonance (SPR) of the green synthesized AgNPs solution was measured using Systronics 117 UV-Visible spectrophotometer. Fourier transform infrared (FT-IR) spectrum of Avocado leaf extract mediated silver nanoparticles was obtained in the range of 4000 to 400 cm^{-1} with a Thermoscientific NicoletiS50 spectrophotometer. The nonlinear optical studies were carried out using a single beam Z-scan setup with a 532 nm Nd: YAG (SHG) pulsed laser beam focused by a lens of 15 cm focal length.

RESULTS AND DISCUSSION

X-ray diffraction studies: The X-ray diffraction patterns reveal the well-defined crystalline nature of the crystals. Fig. 1 shows the XRD pattern with the diffraction peaks at 38.11º, 44.26º, 64.42º and 77.47º corresponding to (1 1 1), (2 0 0), (2 2 0) and (3 1 1) facets of the face-centered cubic crystal structure. The data obtained which is helpful for analysis having peaks corresponding to different planes of crystal are well matched to standard PDF data (card No:87-0720) for the cubic phase of silver. An average crystallite size of 11 nm was obtained when calculated using the Debye-Scherrer equation [5,6]:

$$D = \frac{K\lambda}{\beta \cos\theta} \quad (1)$$

where D is the crystallite size of AgNPs; λ is the wavelength of the X-ray source (0.1541 nm); β is the full width at half maximum of the diffraction peak; K is the Scherrer constant with a value from 0.9 to 1; and θ is the Bragg angle. In addition to the respective peaks of fcc silver nanocrystals, additional unassigned peaks were also observed suggesting that the crystallization of the bioorganic phase occurs on the surface of the AgNPs due to the aqueous leaf extract [24].

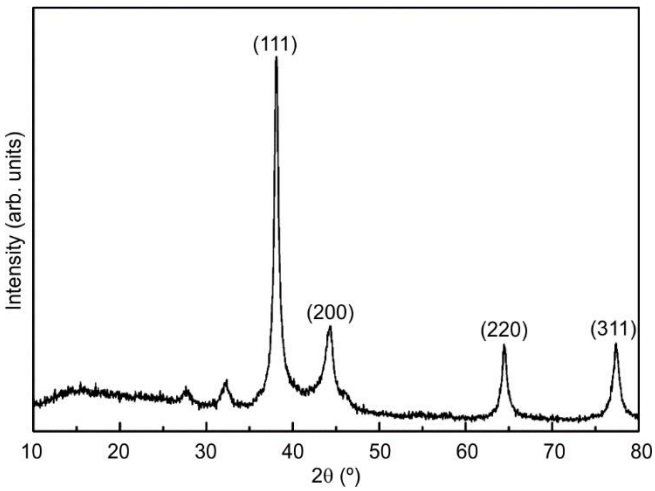

Fig. 1. X-ray diffraction pattern of as-synthesized AgNPs

UV-visible spectral studies: The formation of AgNPs was analyzed using UV-Vis absorption spectroscopy. Silver nanoparticles exhibit a yellowish-brown colour due to the excitation of surface plasmon vibrations in the metal nanoparticles [25,26]. The UV-visible absorption spectrum of AgNPs was recorded from 200-1100 nm and is shown in Fig. 2. The location of AgNPs SPR band was found to be around 452 nm and the occurrence of this peak was due to the size of AgNPs.

FTIR spectral studies: The FTIR spectrum of green synthesized AgNPs using avocado leaf extract typically shows the characteristic peaks that can be attributed to the functional groups present in the leaf extract, as well as those involved in

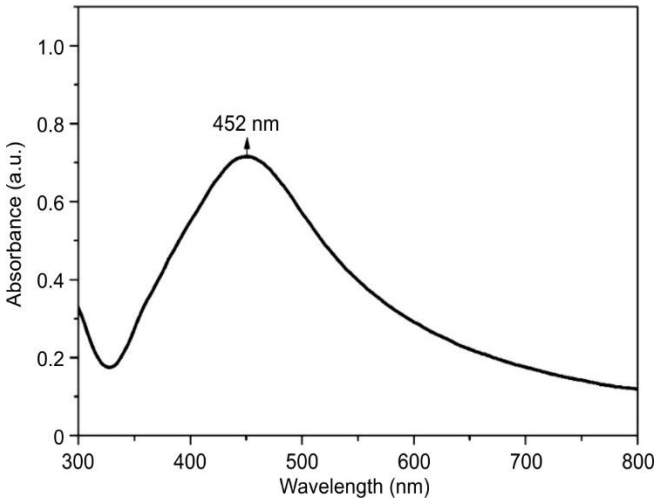

Fig. 2. UV-vis absorption spectrum of as-synthesized AgNPs

the reduction and stabilization of the silver nanoparticles. Fig. 3 shows the FTIR spectra of the synthesized silver nanoparticles. A broad peak near ~3400 cm^{-1} corresponds to O-H stretching vibrations, indicating the presence of hydroxyl groups. These groups likely originate from phenolic compounds, alcohols or water molecules involved in the capping and stabilization of the nanoparticles. The spectrum also displays absorption peaks at 2981, 1611, 1382 and 1151 cm^{-1}, respectively. The peak at 2981 cm^{-1} relates to C-H stretching vibrations, which suggest the presence of aliphatic or aromatic hydrocarbons. These may originate from organic compounds found in the avocado leaf extract. The peak at 1611 cm^{-1} is linked to C=O stretching vibrations of carbonyl groups. This implies the presence of amides, carboxylic acids or ketones, which may assist in stabilizing and capping the nanoparticles. The peak around ~1382 cm^{-1} implies symmetric or asymmetric bending of CH_3 or CH_2 groups, likely associated with proteins or amino acids that facilitate stabilization. The peaks at 1151 cm^{-1} indicate C-O stretching, which could suggest the existence of alcohols, esters, or polysaccharides that contribute to the stabilization of the nanoparticles. Hence, the FTIR spectrum shows the participation of biomolecules from

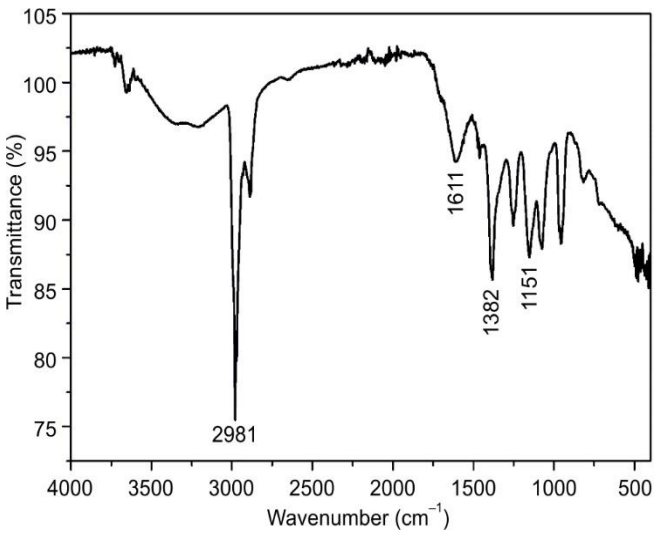

Fig. 3. FTIR spectrum of as-synthesized AgNPs

the avocado leaf extract (like flavonoids, phenolics, proteins and carbohydrates) in the reduction and stabilization of silver nanoparticles [20].

Antibacterial activity: The antibacterial activity of biogenic AgNPs against *Proteus mirabilis* bacterial strains (sourced from Department of Microbiology at Micro Labs, Kozhencherry, carried out at PG and Research Department of Zoology, NSS College, Pandalam) was examined using the agar diffusion method in the Muller-Hinton agar medium. The bacteria were cultivated for 24 h in nutrient broth before being aseptically spread onto solidified Mueller-Hinton agar plates using a sterilized cotton swab following the pour plate technique. Wells of equal distance and equal diameter (4 mm) were made by sterilized gel borer. Each well was filled with 20 µL of synthesized AgNP suspensions of three concentrations 25 µg/10 mL, 50 µg/10 mL and 75 µg/10 mL. The plates were kept for incubation at 30 ºC for 24 h. The sensitivities of the test organisms to the different concentrations were indicated by the formation of clear zones with dimensions around 11 mm around the wells, as shown in Fig. 4.

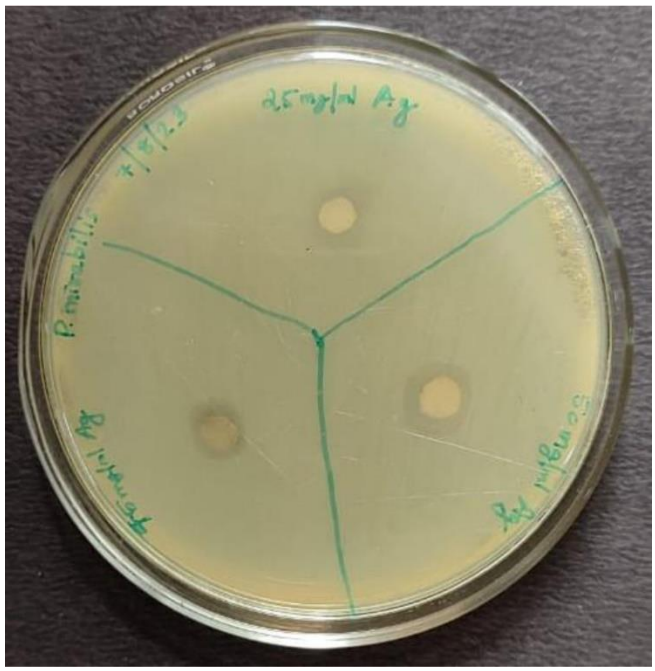

Fig. 4. Inhibition zone of AgNPs against *P. mirabilis* pathogens

Nonlinear optical studies: The synthesized AgNPs were subjected to nonlinear optical studies using a single-beam Z-scan technique [27]. A lens with a focal length of 28 cm focuses a Gaussian laser beam with a spatial dispersion. The laser beam travels along the z-axis, with z = 0 as its focal point. The laser beam waist, or w_0, at the focus is 3.72×10^{-5} m. There are two modes in the z-scan technique: one is open and the other is closed aperture modes (Fig. 5a-b, respectively). The beam from 532 nm Nd: YAG laser with laser pulses (pulse rate 5 ns) of a low frequency of 10 Hz was focused using a 28 cm focal length lens. A 1mm quartz cuvette containing the samples under investigation was placed on a translation stage and moved across the focal region (+z to –z) along the axial direction, which was the direction of propa-

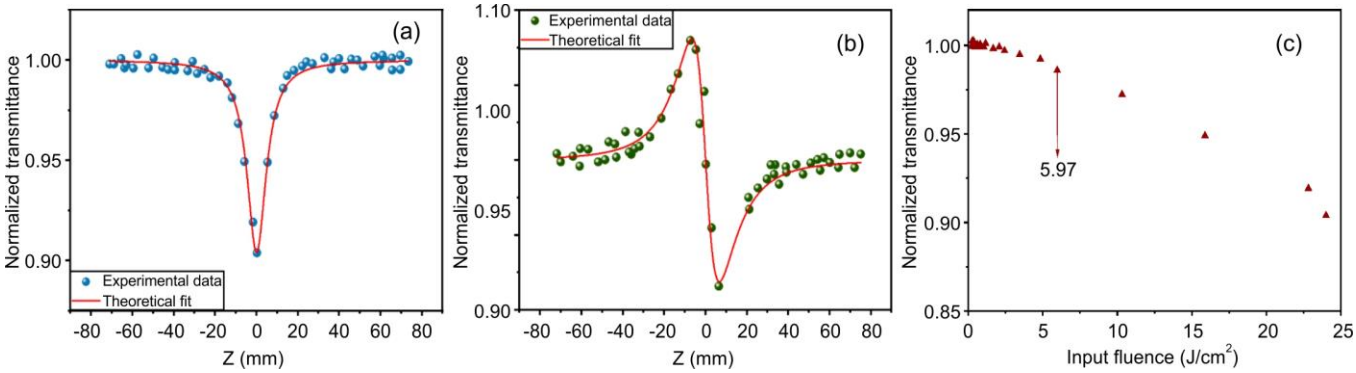

Fig. 5. Open aperture Z-scan curve (a); closed aperture Z-scan curve (b) and the optical limiting behaviour (c) of as-synthesized AgNPs

gation of the laser beam. Fig. 5a shows the open aperture Z-scan measurement of AgNPs. The intensity of the beam transmitted through the nanoparticle solution was collected by a photodetector without an aperture and measured by the digital power meter. By fitting the experimental results to the theoretical model of two-photon absorption, the nonlinear absorption coefficient was found. The open aperture data shows the reverse saturable absorption (RSA) in the AgNPs, which is attributed to the excitations from the SPR band to the free carrier band and also the direct two-photon absorption (TPA) from ground state [28,29].

For obtaining the value of the nonlinear absorption coefficient (β), the obtained open aperture experimental data was fitted using eqn. 2 [30]:

$$T(z) = \left(\sum_{m=0}^{\infty} \frac{\left(\frac{q_0(z)}{\left(1+\frac{z^2}{z_0^2}\right)} \right)^m}{(m+1)^{\frac{3}{2}}} \right) \quad (2)$$

where T(z) represents the normalized transmittance obtained from the open aperture data.

$$q_o = \beta I_0 L_{eff} \quad (3)$$

where 'β' denotes the nonlinear absorption coefficient at the focal point (z = 0) and I_0 is the peak intensity at the focus. The effective thickness of the compound, L_{eff} with linear absorption α and sample length '*l*' is given by eqn. 4 [30]:

$$L_{eff} = \frac{1-e^{-\alpha l}}{\alpha} \quad (4)$$

The value of β directly depends on the imaginary component of the third-order NLO susceptibility [31]:

$$Im(x)^3 = \frac{(\varepsilon_o \chi^2 n_0^2)\beta}{4\pi^2} esu \quad (5)$$

For the closed aperture data, an aperture is placed in front of the detector when using the closed aperture z-scan technique. Refractive nonlinearities can be efficiently measured using the plot that shows the relationship between the amount of light that passes through the aperture and the location of a sample along the z-axis [27,29].

Fig. 5b displays a peak-valley pattern, which is characteristic of a closed-aperture Z-scan experiment. The experimental data is indicated by the green points, while the red line represents the theoretical fit to this data. The peak observed on the left (positive Z values) along with the valley on the right (negative Z values) implies a negative nonlinear refractive index (n_2) of the material, suggesting that the material possesses self-defocusing characteristics. In the self-defocusing phenomenon, the refractive index diminishes as light intensity increases. The Y-axis illustrates normalized transmittance, depicting the amount of light that transmits through the sample at various locations along the Z-axis. The changes in transmittance arise from variations in the optical path length caused by the nonlinear refractive index.

In the open aperture approach, only the nonlinear absorption behaviour is detected by the transmittance. Removing the aperture causes the transmittance to lose sensitivity to any beam distortion [27]. The intensity-dependent refractive index of a material (refractive index modulation) can be expressed as follows:

$$n(I) = n_0 + n_2 I \quad (6)$$

To obtain the value of n_2 the closed aperture experimental data is fitted using the following equation [30]:

$$T(z, \Delta\phi_0) = \frac{1-4\Delta\phi_0 x}{(x^2+9)(x^2+1)} \quad (7)$$

where $x = z/z_0$, T denotes the normalized transmittance found from the closed aperture z-scan technique and $\Delta\phi_0$ nonlinear phase shift occurring at the focal point. The value of the nonlinear index of refraction is estimated from eqn. 8:

$$\Delta\phi_0 = k n_2 I_0 L_{eff} \quad (8)$$

where the wave vector (k) has a value of $2\pi/\lambda$. The value of n_2 is directly related to the real component of third-order NLO susceptibility of the material [30]:

$$Re(x)^3 = \frac{(\varepsilon_0 n_0^2 c^2) n_2 10^{-4}}{\pi} esu \quad (9)$$

Optical limiting: To investigate the optical power limiting behaviour of the compounds, the laser pulse energy per effective focal spot area, referred as laser fluence (J/cm^2), was calculated from the open aperture data and plotted against the normalized transmittance. The sample was subjected to varying laser fluence levels at different positions along the Z-axis, with maximum intensity at the focal point. The position-dependent laser fluence was determined using the eqns 10 and 11 [30]:

TABLE-1
OBTAINED VALUES OF NONLINEAR OPTICAL PARAMETERS OF SYNTHESIZED SILVER NANOPARTICLES

Input intensity (mJ)	β ($\times 10^{-9}$ cm/W)	n_2 ($\times 10^{-15}$ cm^2/W)	Re($\chi^{(3)}$) ($\times 10^{-13}$ esu)	Im($\chi^{(3)}$) ($\times 10^{-13}$ esu)	$\chi^{(3)}$ ($\times 10^{-13}$ esu)	OL threshold (J/cm^2)
0.5	1.8385	1.491	5.044	2.635	5.6907	5.97

$$F(z) = \frac{4\sqrt{\ln 2}(E_{in})}{(\pi^{3/2})\omega(z)^2} \quad (10)$$

$$\omega(z) = \omega(0)\sqrt{1+\left(\frac{z}{z_0}\right)^2} \quad (11)$$

where F(z) refers to the laser input fluence at sample position z; ω(z) represents the beam waist radius corresponding to each z position and E_{in} is the laser input energy.

Table-1 shows the calculated values of third-order nonlinear optical parameters of the synthesized AgNPs. The optical threshold corresponds to the light intensity at which the optical limiting effect becomes significant and the transmission of light starts to reduce as the intensity increases. This threshold can be determined from the Z-scan data by analyzing the point where the transmission begins to drop as a function of the laser intensity [32,33]. Green synthesized AgNPs exhibit significant optical limiting properties due to their nonlinear optical behaviour. When synthesized using plant extracts (such as avocado leaf extract), AgNPs not only retain their desirable plasmonic properties but may also have enhanced or tunable optical responses due to the interaction with organic molecules from the extract. Fig. 5c presents the optical limiting behaviour of AgNPs, where at lower light intensities, the AgNPs exhibit minimal attenuation and allow greater light transmission. However, as the light intensity increases beyond a certain threshold, the nanoparticles begin to exhibit stronger absorption, reducing the transmission and effectively limiting the optical power passing through. No further increase in output was observed with increasing input beam intensity, confirming the optical limiting behaviour of the as-synthesized particles [31].

Conclusion

Highly stable silver nanoparticles (AgNPs) were synthesized utilizing a straightforward, economical and environmental friendly method that employed leaf extract from the *Persia americana* (avocado), as stabilizing and reducing agent. The as-produced AgNPs have an average size of about 11 nm with face face-centred cubic crystal structure. The prepared silver nanoparticles were subjected to nonlinear optical behaviour studies by single beam Z-scan setup. The synthesized AgNPs show good antimicrobial effects against human pathogens *P. mirabilis* and have good nonlinear optical behaviour. The AgNPs showed better optical limiting properties with a threshold value of 5.97 J/cm^2, indicating biogenic AgNPs as potential candidates for optoelectronic devices and applications.

ACKNOWLEDGEMENTS

The authors thank the Department of Nanoscience and Nanotechnology, University of Kerala, for conducting NLO studies. The authors also acknowledge CLIF, University of Kerala, Research Department of Physics and Department of Zoology, N.S.S. College, Pandalam, for providing the necessary facilities.

CONFLICT OF INTEREST

The authors declare that there is no conflict of interests regarding the publication of this article.

REFERENCES

1. M. Nidya, M. Umadevi, P. Sankar, R. Philip and B.J.M. Rajkumar, *Opt. Mater.*, **42**, 152 (2015); https://doi.org/10.1016/j.optmat.2015.01.002
2. S. Pugazhendhi, P. Sathya, P.K. Palanisamy and R. Gopalakrishnan, *J. Photochem. Photobiol. B*, **155**, 5 (2016); https://doi.org/10.1016/j.jphotobiol.2016.03.043
3. K. Shameli, M. Ahmad, P. Shabanzadeh, A. Zamanian, P. Sangpour, Y. Abdollahi and Z. Mohsen, *Int. J. Nanomedicine*, **2012**, 5603 (2012); https://doi.org/10.2147/IJN.S36786
4. G. Karunakaran, M. Jagathambal, A. Gusev, E. Kolesnikov, A.R. Mandal and D. Kuznetsov, *MRS Commun.*, **6**, 41 (2016); https://doi.org/10.1557/mrc.2016.2
5. D.-M. Radulescu, V.-A. Surdu, A. Ficai, D. Ficai, A.-M. Grumezescu, and E. Andronescu, *Int. J. Mol. Sci*., **24**, 15397 (2023); https://doi.org/10.3390/ijms242015397
6. N. Ahmad, S. Sharma, M.K. Alam, V.N. Singh, S.F. Shamsi, B.R. Mehta and A. Fatma, *Colloids Surf. B Biointerfaces*, **81**, 81 (2010); https://doi.org/10.1016/j.colsurfb.2010.06.029
7. A. Nabikhan, K. Kandasamy, A. Raj and N.M. Alikunhi, *Colloids Surf. B Biointerfaces*, **79**, 488 (2010); https://doi.org/10.1016/j.colsurfb.2010.05.018
8. I.J. Lithi, K.I.A. Nakib, A.M.S. Chowdhury and M.S. Hossain, *Nanoscale Adv.*, **7**, 2446 (2025); https://doi.org/10.1039/D5NA00037H
9. N. Revathi, M. Sankarganesh, J. Dhaveethu Raja, J. Rajakanna and O. Senthilkumar, *Inorg. Chem. Commun.*, **154**, 110935 (2023); https://doi.org/10.1016/j.inoche.2023.110935
10. S. Shahzadi, S. Fatima, Q. ul Ain, Z. Shafiq and M.R.S.A. Janjua, *RSC Adv.*, **15**, 3858 (2025); https://doi.org/10.1039/D4RA07519F
11. H. Chopra, S. Bibi, I. Singh, M.M. Hasan, M.S. Khan, Q. Yousafi, A.A. Baig, M.M. Rahman, F. Islam, T.B. Emran and S. Cavalu, *Front. Bioeng. Biotechnol.*, **10**, 874742 (2022); https://doi.org/10.3389/fbioe.2022.874742
12. F. Khan, M. Shariq, M. Asif, M. A. Siddiqui, P. Malan and F. Ahmad, *Nanomaterials*, **12**, 673 (2022); https://doi.org/10.3390/nano12040673
13. F. Ahmadi and M. Lackner, *Chem. Eng.*, **8**, 64 (2024); https://doi.org/10.3390/chemengineering8040064
14. S. Iravani, *Green Chem.*, **13**, 2638 (2011); https://doi.org/10.1039/C1GC15386B
15. S. Pugazhendhi, E. Kirubha, P.K. Palanisamy and R. Gopalakrishnan, *Appl. Surf. Sci.*, **357**, 1801 (2015); https://doi.org/10.1016/j.apsusc.2015.09.237
16. F.Z. Henari and H. Manaa, *Opt. Photonics J.*, **8**, 235 (2018); https://doi.org/10.4236/opj.2018.87020
17. N.U.H.H. Zalkepali, T.J. Sang, T.J. Xuan, A.Z.M. Zamri, N.N.H.E.N. Mahmud, K.L. Mun and N.A. Awang, *Opt. Fiber Technol.*, **87**, 103915 (2024); https://doi.org/10.1016/j.yofte.2024.103915

18. Y. Wang, X. Li, A. Wang, J. Zhang, J. Wo and Q. Wang, *Am. J. Opt. Photon.*, **9**, 18 (2021); https://doi.org/10.11648/j.ajop.20210901.13
19. H. Qayyum, S. Mamdouh, A. Mahmoud and T. Mohamed, *Laser Innov. Res. Appl.*, **2**, 1 (2025); https://doi.org/10.21608/lira.2025.383757.1007
20. F. Anjum, A. Saddiq, M. M. Nazir, R. Naseer, M. Riaz and A. Ashraf, *Int. J. Biol. Macromol.*, **329**, 147771 (2025); https://doi.org/10.1016/j.ijbiomac.2025.147771
21. Y. Ngungeni, J.A. Aboyewa, K.L. Moabelo, N.R.S. Sibuyi, S. Meyer, M.O. Onani, M. Meyer and A.M. Madiehe, *ACS Omega*, **8**, 26088 (2023); https://doi.org/10.1021/acsomega.3c02260
22. O. Al-Hammood, S.H. AlRajhi, A.G. Oraibi and M. Kadhom, *Results Chem.*, **12**, 101895 (2024); https://doi.org/10.1016/j.rechem.2024.101895
23. B. Kumar, K. Smita, A. Debut and L. Cumbal, *Environ. Nanotechnol. Monit. Manag.*, **10**, 231 (2018); https://doi.org/10.1016/j.enmm.2018.07.009
24. M.M. Khalil, E.H. Ismail, K.Z. El-Baghdady and D. Mohamed, *Arab. J. Chem.*, **7**, 1131 (2014); https://doi.org/10.1016/j.arabjc.2013.04.007
25. P. Papolu and A. Bhogi, *Mater. Today Proc.*, **92**, 924 (2023); https://doi.org/10.1016/j.matpr.2023.04.544
26. P. Mulvaney, *Langmuir*, **12**, 788 (1996); https://doi.org/10.1021/la9502711
27. M. Sheik-Bahae, A.A. Said, T.H. Wei, D.J. Hagan and E.W. Van Stryland, *IEEE J. Quantum Electron.*, **26**, 760 (1990); https://doi.org/10.1109/3.53394
28. F.Z. Henari and H. Manaa, *Opt. Photon. J.*, **8**, 235 (2018); https://doi.org/10.4236/opj.2018.87020
29. S. Chitrambalam, S. Abraham, V.K. Rastogi and I.H. Joe, *Chem. Phys. Lett.*, **754**, 137648 (2020); https://doi.org/10.1016/j.cplett.2020.137648
30. A.A. Noble and I.H. Joe, *Surf. Interfaces*, **44**, 103603 (2024); https://doi.org/10.1016/j.surfin.2023.103603
31. K. Ozga, M. Oyama, M. Szota, M. Nabiałek, I.V. Kityk, A. Ślęzak, A.A. Umar and K. Nouneh, *J. Alloys Compd.*, **509**, S424 (2011); https://doi.org/10.1016/j.jallcom.2010.12.107
32. P. Chantharasupawong, R. Philip, N.T. Narayanan, P.M. Sudeep, A. Mathkar, P.M. Ajayan and J. Thomas, *J. Phys. Chem. C*, **116**, 25955 (2012); https://doi.org/10.1021/jp3096693
33. D. Dini, M.J.F. Calvete and M. Hanack, *Chem. Rev.*, **116**, 13043 (2016); https://doi.org/10.1021/acs.chemrev.6b00033